Structure and stability of superfluid ^{4}He systems with cylindrical symmetry

Leszek Szybisz[1,2,*] and Silvina M. Gatica[2,*]
[1]*Laboratorio TANDAR, Departamento de Física, Comisión Nacional de Energía Atómica, Avenida del Libertador 8250, RA-1429 Buenos Aires, Argentina*
[2]*Departamento de Física, Facultad de Ciencias Exactas y Naturales, Universidad de Buenos Aires, Ciudad Universitaria, RA-1428 Buenos Aires, Argentina*

(Received 29 December 2000; revised manuscript received 8 June 2001; published 26 November 2001)

The structure and stability of superfluid ^{4}He systems with cylindrical symmetry are studied. Ground-state energies and density profiles are computed by using density-functional approaches. A model to understand the energetics of cylindrical systems is developed by following the main ideas of the Droplet Model utilized to describe spherical clusters. The necessary condition for stability is formulated by imposing a positive longitudinal isothermal compressibility along the principal axis of the cylinder. It is shown that free cylinders of ^{4}He at $T=0$ K are unstable. As an example of the evolution towards stable systems, results for liquid ^{4}He confined by cylindrical nanopores in Cs are reported.

DOI: 10.1103/PhysRevB.64.224523 PACS number(s): 61.20.−p, 68.03.Cd

I. INTRODUCTION

The investigation of properties of superfluid helium adsorbed in porous materials has long been a subject of interest. A pioneering study of Vycor (glass, 99% of SiO_2) was performed by Atkins, Seki, and Condon[1] in 1956 for testing the onset of superfluid flow. Since that time an important research activity has been developed in this field. An important theoretical work on this matter has been done by Cole and Saam.[2,3] These authors have derived a formulation based on the thermodynamics and hydrodynamic theory of fluid systems in order to study ^{4}He adsorbed on the internal wall of cylindrical pores. A survey of subsequent experimental work on the helium adsorption into Vycor, Graphfoil (graphene foil), and Nucleopore (polycarbonate) may be found in the work of Godshalk and Hallock[4] and references quoted therein. More recently, during the last decade the effort has been mainly centered round the study of the adsorption of helium in carbon nanotubes.[5–9] Let us emphasize that the graphite wall of the nanotube exerts an extremely strong attraction on helium atoms. On the other hand, hitherto no attention has been paid in the literature to ^{4}He adsorbed into weakly attractive cylindrical pores, which could be present in samples of alkali metals. Adsorption on planar surfaces of this kind of metals has already been extensively studied[10–16] leading to the important conclusion that the less attractive alkali, Cs, is not wet by ^{4}He at temperatures $T \lesssim 2$ K.[17] All these facts have encouraged us to start an investigation of the behavior of ^{4}He adsorbed into nanopores in alkali metals.

In the present work, we shall report the investigation about the behavior of ^{4}He adsorbed into cylindrical nanopores in the ultra-weakly attractive substrate of Cs. To illustrate our findings, the results for two different pore sizes of radii 3 and 5 nm will be shown and discussed.

The calculations for the ground state have been carried out within the density-functional (DF) theory. This formalism has proven to be a successful tool for treating this kind of quantum many-body problems.[18–28] Let us mention that the formulation of the energy of a given system in the DF theory[22] differs from that assumed in the hydrodynamic theory used in the above-mentioned paper of Cole and Saam.[2,3] In our study the ground-state energy E_{gs} of an interacting N-body bosonic system of ^{4}He atoms confined by a adsorbate-substrate potential $U_{sub}(\mathbf{r})$ was written as

$$E_{gs} = \int d\mathbf{r}\rho(\mathbf{r})\mathcal{H}[\rho,\nabla\rho] + \int d\mathbf{r}\rho(\mathbf{r})U_{sub}(\mathbf{r})$$
$$= -\frac{\hbar^2}{2m}\int d\mathbf{r}\sqrt{\rho(\mathbf{r})}\nabla^2\sqrt{\rho(\mathbf{r})}$$
$$+ \int d\mathbf{r}\rho(\mathbf{r})e_{sc}(\mathbf{r}) + \int d\mathbf{r}\rho(\mathbf{r})U_{sub}(\mathbf{r}), \qquad (1.1)$$

where $\rho(\mathbf{r})$ is the one-body density. The first term on the right-hand side is the quantum kinetic energy of the helium particles of mass m. The second term represents the interaction between the particles of the system, where $e_{sc}(\mathbf{r})$ is the self-correlation energy per particle depending on the adopted DF approach. The last term is the interaction with the external field.

The optimal solution is obtained by minimizing the thermodynamic grand potential Ω,

$$\Omega = E_{gs}[\rho,\nabla\rho] - \mu N, \qquad (1.2)$$

at fixed chemical potential μ, i.e., by requiring

$$\left(\frac{\partial\Omega}{\partial N}\right)_{\mu} = \frac{\partial E_{gs}[\rho,\nabla\rho]}{\partial N} - \mu = 0. \qquad (1.3)$$

In practice, the Euler-Lagrange (EL) equation for determining the density profile $\rho(\mathbf{r})$ is derived imposing the variational condition

$$\frac{\delta\Omega}{\delta\rho(\mathbf{r})} = \frac{\delta\{E_{gs}[\rho,\nabla\rho] - \mu N\}}{\delta\rho(\mathbf{r})} = 0. \qquad (1.4)$$

Let us mention in passing, that in order to study ^{3}He systems the kinetic-energy term in Eq. (1.1) must be modified due to the fact that fermions obey a different statistics (see, e.g., Refs. 19 and 29). Furthermore, the optimization equation in the case of ^{3}He becomes more complicated than Eq. (1.4)

because the corresponding one-body density $\rho(\mathbf{r})$ must be expanded in an appropriate single-particle basis [cf. Eq. (3.5) in Ref. 21].

In the route to analyze weakly attractive pores we shall first examine free cylindrical systems of ^{4}He. It is known that free spherical drops of ^{4}He at $T=0$ K are always stable,[18,30] while to the contrary free planar films are unstable against long-wavelength fluctuations.[26,27] Long time ago it has been found by Rayleigh that the surface of a perfect free cylinder of fluid is intrinsically unstable because there are other geometries of lower surface areas yielding lower interfacial free energies. In particular, the cylindrical geometry is not stable relative to the spherical one because the latter geometry have a lower surface/volume ratio. The reader may find a discussion of this issue in Ref. 31. In this context, it is worthwhile to complete the pattern within microscopic theories obtained for regular geometries by studying the stability of free cylinders of ^{4}He.

In fact, there are two different ways for establishing the necessary condition for the stability of a given system.[26,27] One of them is based on a study of the excitation spectrum of the analyzed system and leads to the so called dynamical condition. In the framework of the DF theory the latter kind of procedure requires the solution of an eigenvalue problem [see Eq. (2.7) in Ref. 32] formally equivalent to that of the hydrodynamic theory [see Eq. (3.2) of Ref. 3]. To get dynamic stability one must require that the lowest eigenvalue $\hbar^2\omega_0^2$ be positive. The other way consists of a study of the energetics within a thermodynamic description.[33] In this case one has to analyze the evolution of the grand thermodynamic potential Ω of samples with increasing number of particles N. The requirements for stability are: (i) that $\Omega(N)$ be lower than that of any smaller system even than that of all other configurations and (ii) that the slope of the chemical potential $d\mu/dN$ in the neighborhood of the analyzed system be positive. However, it has been shown by Clements *et al.* that in case of the DF theory the thermodynamic and dynamic instability conditions are rigorously identical [see comment to Eqs. (5.2) and (5.3) in Ref. 32]. Furthermore, the authors of Ref. 2 have also stated that the thermodynamic instability condition is identical to the dynamical stability limit obtained within the hydrodynamic theory [see the comment to Eq. (8) therein]. In practice, one may find a situation where dynamic stability is accompanied by thermodynamic metastability. It occurs when both $\hbar^2\omega_0^2$ and $d\mu/dN$ are positive but $\Omega(N)$ does not satisfy the condition (i). In the present work we shall examine the stability applying the thermodynamic criterion.

The paper is organized in the following way. The adopted DF approaches are outlined in Sec. II. Numerical results are provided in Sec. III. A model for interpreting the results exhibiting a well-defined axial phase is proposed in Sec. IV. Section V is devoted to study thermodynamic properties and to formulate a stability criterion. The analysis and discussion are performed in Sec. VI and a summary is given in Sec. VII.

II. THEORETICAL APPROACHES

In this work we report results of calculations performed by using two different DF approaches for ^{4}He systems, namely, the Skyrme-type ''zero-range'' expression suggested in Ref. 19 and the nonlocal density functional (NLDF) formalism proposed in Ref. 20 (the versions of these DF adequate for studying ^{3}He may be found in Refs. 19 and 21, respectively).

In the cylindrical geometry, the fluid is translationally invariant along the coordinate z coincident with the principal axis of the cylinder and exhibits a density profile in the radial direction r perpendicular to z. So, in this case, the liquid ^{4}He is confined by the action of supporting potentials of the form $U_{\rm sub}(\mathbf{r})\equiv U_{\rm sub}(r)$ independent of the azimuthal angle φ. The quantities of interest were obtained from the solution of the Hartree equation for the square root of the one-body density [derived by using Eq. (1.4)]

$$-\frac{\hbar^2}{2m}\left(\frac{d^2}{dr^2}+\frac{1}{r}\frac{d}{dr}\right)\sqrt{\rho(r)}+[V_H(r)+U_{\rm sub}(r)]\sqrt{\rho(r)} =\mu\sqrt{\rho(r)}, \tag{2.1}$$

which also determines μ. Here $V_H(r)$ is a Hartree mean-field potential given by the first functional derivative of the total correlation energy $E_{sc}[\rho]$,

$$V_H(r)=\frac{\delta E_{sc}[\rho]}{\delta\rho(r)}=\frac{\delta}{\delta\rho(r)}\int d\mathbf{r}'\,\rho(r')e_{sc}(\mathbf{r}'). \tag{2.2}$$

The expressions for $V_H(r)$ should be derived for each one of the different DF approaches. In practice, Eq. (2.1) is solved for a given number of particles N per unit length L along the z axis, i.e., at fixed $n_\lambda=N/L$.

A. Zero-range density functional

The simplest DF successfully employed to interpret properties of ^{4}He systems has been proposed by Stringari and Treiner.[18,19] It is a zero-range correlation inspired in functionals derived by using a phenomenological interaction of Skyrme type, which have been extensively applied to describe properties of atomic nuclei. The explicit form of the correlation energy per particle for cylindrical geometry is

$$e_{sc}^{\rm Sky}(r)=\frac{b_4}{2}\rho(r)+\frac{c_4}{2}\rho^{\gamma_4+1}(r)+d_4\frac{1}{\rho(r)}\left(\frac{d\rho(r)}{dr}\right)^2. \tag{2.3}$$

The phenomenological parameters b_4, c_4, γ_4, and d_4 fixed in Ref. 19 (see Table I therein) so as to reproduce the known saturation properties of the uniform liquid (i.e., the equilibrium density, the energy per particle, the compressibility, and the surface tension quoted in Table I) are

$$\begin{aligned} b_4&=-8.888\,10\times10^2\ \ \mathrm{K\,\AA^3},\\ c_4&=1.045\,54\times10^7\ \ \mathrm{K\,\AA^{3(\gamma_4+1)}},\\ \gamma_4&=2.8,\\ d_4&=2.383\times10^3\ \ \mathrm{K\,\AA^5}. \end{aligned} \tag{2.4}$$

The corresponding $V_H^{\rm Sky}(r)$ is given in the Appendix.

TABLE I. Bulk observables, experimental values of the surface tension for liquid ^{4}He at $T=0$, and values of the LJ parameters.

Observable	Data		Ref.
e_B [K]	-7.15		19
ρ_0 [Å^{-3}]	0.021836		19
$\mathcal{K}$ [K]	27.2		19
$\sigma_{\rm exp}$ [K/Å^2]	0.274 ± 0.003		38
	0.257 ± 0.001		39
	0.272 ± 0.002		40
System	ε_{LJ} [K]	σ_{LJ} [Å]	
He-He	10.22	2.556	34
He-Cs	1.21	6.47	41

B. Orsay-Paris nonlocal density functional

The Orsay-Paris nonlocal functional (OP-NLDF) proposed by Dupont-Roc *et al.*,[20] which treats correctly the long-range part of the helium-helium interaction and improves the description of correlations, is sufficiently good to reproduce properties of nonlayered systems like free or weakly confined cylindrical systems. This functional reads

$$e_{sc}^{\rm OP}(\mathbf{r})=\frac{1}{2}\int d\mathbf{r}'\rho(\mathbf{r}')V_l^{\rm OP}(|\mathbf{r}-\mathbf{r}'|)+\frac{c_4}{2}[\overline{\rho}(\mathbf{r})]^{\gamma_4+1}. \tag{2.5}$$

In this case the two-body interaction, $V_l^{\rm OP}(r=|\mathbf{r}-\mathbf{r}'|)$, was taken as the ^{4}He-^{4}He Lennard-Jones (LJ) potential screened in a simple way at distances shorter than a characteristic distance $h_{\rm OP}$,

$$V_l^{\rm OP}(r)=\begin{cases} 4\varepsilon_{LJ}\left[\left(\dfrac{\sigma_{LJ}}{r}\right)^{12}-\left(\dfrac{\sigma_{LJ}}{r}\right)^{6}\right], & \text{if} \quad r\geqslant h_{\rm OP}, \\ V_l^{\rm OP}(h_{\rm OP})\left(\dfrac{r}{h_{\rm OP}}\right)^4, & \text{if} \quad r<h_{\rm OP}, \end{cases} \tag{2.6}$$

with the standard de Boer and Michels[34] parameters, well depth ε_{LJ} and hard core radius σ_{LJ} listed in Table I. In order to recover the correct results for bulk liquid, the screening distance $h_{\rm OP}(=2.376\,728$ Å) has been adjusted[28] so that the integral of $V_l^{\rm OP}(r)$ over the whole three-dimensional space

$$\int d\mathbf{r}V_l^{\rm OP}(r)=\frac{32\pi}{21}\varepsilon_{LJ}\sigma_{LJ}^3\left[\frac{8}{3}\left(\frac{\sigma_{LJ}}{h_{\rm OP}}\right)^9-5\left(\frac{\sigma_{LJ}}{h_{\rm OP}}\right)^3\right], \tag{2.7}$$

be equal to the value of b_4 quoted in Eq. (2.4).

The $\overline{\rho}(\mathbf{r})$ is the ''coarse-grained density'' defined as the straight average of $\rho(\mathbf{r})$ over a sphere centered at $\mathbf{r}$ and with a radius equal to the screening distance $h_{\rm OP}$,

$$\overline{\rho}(\mathbf{r})=\int d\mathbf{r}'\rho(\mathbf{r}')\mathcal{W}(|\mathbf{r}-\mathbf{r}'|), \tag{2.8}$$

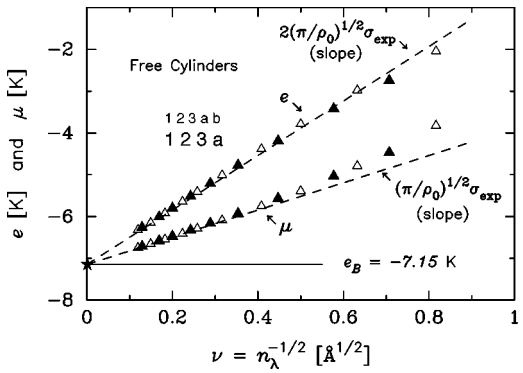

FIG. 1. Energy per particle and chemical potential as a function of the inverse of square root of longitudinal density $\nu=n_\lambda^{-1/2}$ for free cylinders of ^{4}He. Results obtained with the Skyrme-DF and OP-NLDF approaches are represented by open and full triangles, respectively. The dashed lines are the linear approximations given by Eqs. (3.1) and (3.2) with $\sigma_\infty=\sigma_{\rm exp}=0.272$ K/Å^2 taken from Ref. 40.

where $\mathcal{W}(|\mathbf{r}-\mathbf{r}'|)$ is taken as a normalized step function. The relevant quantities for solving a cylindrical system are summarized in the Appendix.

III. NUMERICAL RESULTS

A. Free cylinders

In the case of free cylinders the integrodifferential problem (2.1) has been solved for a range of n_λ enough to cover the domain of energy per particle $-6\lesssim e\lesssim -2$ K. This regime of e is similar to that utilized for studying free systems with other symmetries (see, e.g., Fig. 3 in Ref. 35 for planar films and Fig. 1 in Ref. 36 for spherical drops). Some selected results for e and μ obtained by carrying out calculations with both the Skyrme-DF and OP-NLDF approaches are displayed in Fig. 1. This drawing indicates that for $\nu=n_\lambda^{-1/2}\leqslant 0.4$ Å$^{1/2}$ the data agree very well with the asymptotic limit of expressions derived in the first approach to this problem[37]

$$e=e_\infty+2\sigma_\infty\sqrt{\frac{\pi}{\rho_0}}n_\lambda^{-1/2}, \tag{3.1}$$

and

$$\mu=e_\infty+\sigma_\infty\sqrt{\frac{\pi}{\rho_0}}n_\lambda^{-1/2}, \tag{3.2}$$

where e_∞ is identified with the energy per particle of infinite uniform helium matter at saturation $e_B=E_B/N$ and σ_∞ with the experimental surface tension $\sigma_{\rm exp}$,[38–40] the corresponding values are quoted in Table I. Figure 2(a) shows the evolution of density profiles for increasing n_λ obtained with both utilized functionals. A direct comparison is performed for the system with $n_\lambda=30$ Å^{-1}. In this case the corresponding $V_H(r)$ are plotted in Fig. 2(b). It can be realized that the Hartree mean-field potential yielded by the Skyrme-DF resembles a square-well potential with a small diffusiveness, while the OP-NLDF approach leads to a self-

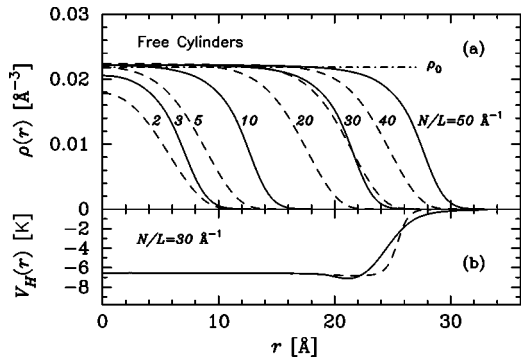

FIG. 2. (a) Density profiles for several free ^{4}He cylinders. The equilibrium saturation density of bulk helium ρ_0 is also indicated. (b) Self-consistent potentials $V_H(r)$ for the system with $n_\lambda = 30$ Å^{-1}. In both parts the solid curves are results obtained with the OP-NLDF approach, while the dashed ones correspond to solutions yielded by the Skyrme-DF.

consistent potential with a more extended structure at the surface region due to the long-range tail proportional to r^{-6} of the Lennard-Jones interaction. This difference causes the small difference in the width of the corresponding profiles displayed in Fig. 2(a). On the other hand, Fig. 2(a) indicates a squeezing effect where the central density ρ_c is larger than the equilibrium density of bulk helium $\rho_0 = 0.021\,836$ Å^{-3}.[19] In order to understand such a compression we shall, in a next section, improve the model proposed in Ref. 37.

B. ^{4}He adsorbed into Cs nanopores

Since in the literature there is no potential for describing the interaction between helium atoms and the wall of a Cs pore, in a first step, we have modeled such a potential. In doing so, we suppose that a pore gives rise to an $U_{\rm sub}(r)$ equal to the sum of contributions yielded by successive concentric cylindrical Cs shells of radius $R_{\rm shell}$,

$$U_{\rm sub}(r) = \sum_s U_{\rm sub}^{(s)}(r, R_{\rm shell}), \tag{3.3}$$

where r is the distance from the axis of the pore. This procedure has been previously used by Stan and Cole[6] in accounting for the effect produced by multiwall carbon nanotubes. Furthermore, we assume that a ^{4}He atom interacts with a single Cs atom of a shell via an isotropic LJ pair potential with parameters ε_{LJ} and σ_{LJ} quoted in Table I. These values are taken from Ancilotto *et al.*,[41] who determined them by adjusting the He-Cs potential of Patil.[42] The next assumption is the use of an azimuthally and longitudinally averaged potential. Under these conditions, it is possible to demonstrate that the total effect for a single shell is given by [see Eq. (2) in Ref. 6]

$$U_{\rm sub}^{(s)}(r, R_{\rm shell}) = 3\pi\Theta_s\varepsilon_{LJ}\sigma_{LJ}^2\left[\frac{21}{32}\left(\frac{\sigma_{LJ}}{R_{\rm shell}}\right)^{10} M_{11}(x) - \left(\frac{\sigma_{LJ}}{R_{\rm shell}}\right)^4 M_5(x)\right], \tag{3.4}$$

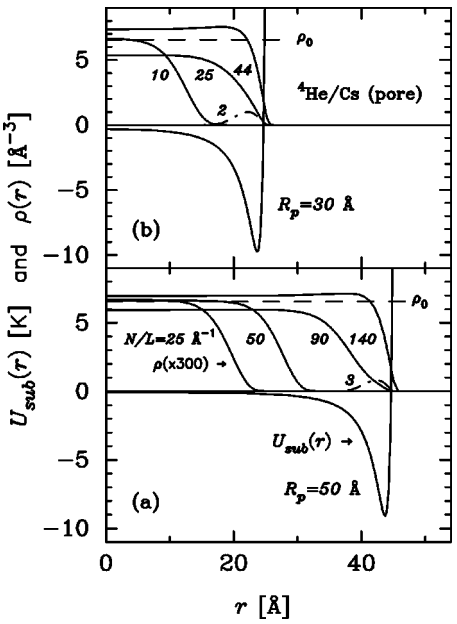

FIG. 3. (a) Adsorbate-substrate potential $U_{\rm sub}(r)$ for the nanopore of $R_p = 50$ Å in Cs given by Eq. (3.4) together with a few selected density profiles of the adsorbed liquid ^{4}He. Solid curves are data of the axial systems with $n_\lambda = 25$, 50, 90, and 140 Å^{-1}, while the dash-dotted curve stands for a shell solution with $n_\lambda = 3$ Å^{-1}. The equilibrium saturation density of bulk helium ρ_0 is also indicated. (b) Similar to part (a) for the pore of $R_p = 30$ Å.

where $x = r/R_{\rm shell}$. In addition, Θ_s is the surface density of Cs atoms and $M_n(x)$ stands for the integrals

$$M_n(x) = \int_0^\pi d\varphi \frac{1}{(1 + x^2 - 2x\cos\varphi)^{n/2}}. \tag{3.5}$$

Quantity Θ_s is determined by taking into account that solid Cs is a bcc crystal with a lattice constant $a = 6.045$ Å taken from Table 3 of Ref. 43. Assuming that each shell coincides with a (100) plane of the crystalline structure of Cs and neglecting effects due to the curvature of the shell, the surface density becomes $\Theta_s = 0.027\,36$ Å^{-2}. The first shell lies at the internal radius of the pore R_p and the subsequent shells are located maintaining a distance $a/2$ between them.

Of course, each approximation performed along this procedure introduces an error. However, we expect that the resulting potential would give a reliable description of the main features of the systems. This statement should be confirmed in the future by *ab initio* calculations.

As specific illustrations we present results for ^{4}He confined by two different cylindrical nanopores of Cs with radii $R_p = 30$ and 50 Å. In both cases the potential converges after summing over fifteen shells. The obtained $U_{\rm sub}(r)$ are displayed in Fig. 3. Notice that both depths are close to ε_{LJ} of the He-He interaction. The repulsive "potential wall" is located at about $R_{\rm rep} = R_p - 5.6$ Å. We solved Eq. (2.1) for these potentials by using both the Skyrme-DF and OP-NLDF proposals. There are not sizable differences between results yielded by these DF approaches.

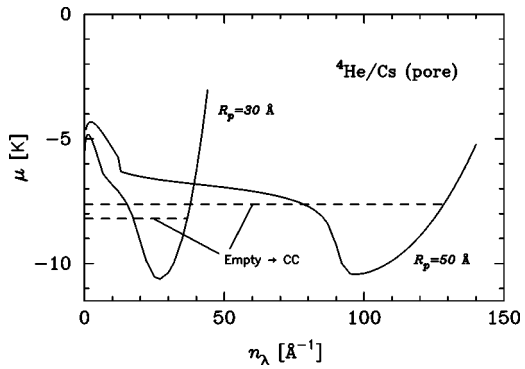

FIG. 4. Chemical potential as a function of the longitudinal density n_λ for ^{4}He in cylindrical pores of radii $R_p=30$ and 50 Å in Cs. The solid curves are OP-NLDF values. Dashed lines are derived by Maxwell constructions for the empty-to-CC transitions.

For very small values of n_λ (less than a few Å^{-1}) there are stable shell solutions similar to that obtained for the adsorption of ^{4}He into carbon nanotubes (see Fig. 10 in Ref. 6), but in the present case the systems are very dilute (gaseous phase not liquid) as can be seen in Fig. 3. For increasing n_λ the shell solution becomes unstable and an axial one develops. This is due to the fact that the attractive correlation between helium atoms becomes stronger than the attraction exerted by the depth of the adsorbate-substrate potential. This transition is a form of capillary condensation (CC).[44] The behavior of the OP-NLDF values of μ as a function of n_λ is depicted in Fig. 4. The results for e and μ corresponding to axial solutions are displayed as a function of $\nu=n_\lambda^{-1/2}$ in Fig. 5. From the latter figure one realizes that, although there are some differences between ^{4}He adsorbed into pores of different R_p, in both cases there is a freelike regime where the data exhibit a slope similar to that obtained for free cylinders. In addition, one may observe that for systems larger than a certain critical n_λ the behavior changes noticeably. Some selected density profiles are given in Fig. 3. Notice that ρ_c of profiles corresponding the freelike regime

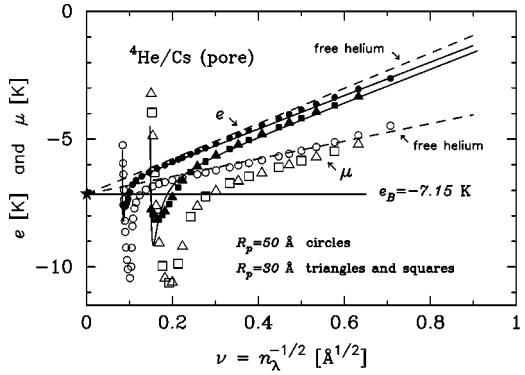

FIG. 5. Energy per particle and chemical potential as a function of the inverse of square root of longitudinal density $\nu=n_\lambda^{-1/2}$ for cylindrical pores of Cs. The full and open circles are OP-NLDF values of e and μ for the pore of radius $R_p=50$ Å. Squares and triangles (full and open) stand for Skyrme-DF and OP-NLDF results (e and μ), respectively, obtained for the pore of radius $R_p=30$ Å. The solid curves are e evaluated with Eq. (6.2).

also present a squeezing effect. In order to continue the discussion of the results we need to introduce some theoretical background.

IV. DROPLETLIKE MODEL FOR CYLINDRICAL SYSTEMS

Let us now describe a formulation for the energetics appropriate for analyzing the axial phase of the solutions. The following formalism is more complete than that of Ref. 37. The equations and discussions reported in this section may be applied to bosonic ^{4}He as well as to fermionic ^{3}He, and even to classical systems. Simple models are often useful for understanding complicated systems. An instructive way to evaluate the energy is to follow the main ideas of the Droplet Model (DM)[45,46] devised for spherical systems. At this point, we shall restrict ourselves to consider free cylinders by setting $U_{\rm sub}(\mathbf{r})=0$. In the case of a large free cylinder, where the length of the principal axis L goes to infinity, the system becomes translationally invariant along the coordinate z and the ground-state energy is

$$E_{\rm gs}=2\pi L\int_0^\infty r\,dr\,\rho(r)\mathcal{H}[\rho,\boldsymbol{\nabla}\rho]. \tag{4.1}$$

Let e_c denote the energy per particle in the central region of the cylinder where the density is ρ_c. Then since

$$N=2\pi L\int_0^\infty r\,dr\,\rho(r), \tag{4.2}$$

we can write the energy as

$$E_{\rm gs}=e_cN+2\pi L\int_0^\infty r\,dr\,\rho(r)\{\mathcal{H}[\rho,\boldsymbol{\nabla}\rho]-e_c\} \tag{4.3}$$

without any approximation or loss of generality. In this procedure the system has been divided into two parts: (i) an uniformly occupied region characterized by the single quantity ρ_c that determines e_c; and (ii) a surface zone where the density falls down. It is easy to realize that the contribution to the integral is localized, since $\rho(r)$ tends to zero outside the surface and $(\mathcal{H}[\rho,\boldsymbol{\nabla}\rho]-e_c)$ tends to zero inside the surface. Because of this property it is convenient to define a sharp mean radius R_s as the radius of a sharp cylindrical uniform distribution of density ρ_c containing all the N particles

$$N=2\pi L\int_0^\infty r\,dr\,\rho_c=\pi R_s^2L\rho_c. \tag{4.4}$$

This definition for R_s coincides with the location of the Gibbs surface. Now one can make the substitution

$$r=R_s+\zeta, \tag{4.5}$$

where ζ is the outward normal distance from the mean surface. After this change of variables one gets

$$E_{\rm gs}=e_cN+2\pi R_sL\int_{-R_s}^{\infty}d\zeta\,\rho(R_s+\zeta)\{\mathcal{H}[\rho,\boldsymbol{\nabla}\rho]-e_c\}$$

$$+2\pi L\int_{-R_s}^{\infty}\zeta d\zeta\,\rho(R_s+\zeta)\{\mathcal{H}[\rho,\boldsymbol{\nabla}\rho]-e_c\}. \quad (4.6)$$

In order to treat large cylindrical systems (in the sense of big sharp mean radius R_s) it is convenient to introduce: (i) the asymptotic surface tension

$$\sigma_\infty=\lim_{R_s\to\infty}\int_{-R_s}^{\infty}d\zeta\,\rho(R_s+\zeta)\{\mathcal{H}[\rho,\boldsymbol{\nabla}\rho]-e_c\}, \quad (4.7)$$

which may be identified with the experimental[38–40] values of the surface tension $\sigma_{\rm exp}$ quoted in Table I; and (ii) the asymptotic energy per unit length

$$\varepsilon_l=2\pi\lim_{R_s\to\infty}\int_{-R_s}^{\infty}\zeta d\zeta\,\rho(R_s+\zeta)\{\mathcal{H}[\rho,\boldsymbol{\nabla}\rho]-e_c\}. \quad (4.8)$$

Under these conditions the ground-state energy of a cylindrical system of N particles may be written as a sum of volume, surface, and length terms

$$E_{\rm gs}=e_cN+\sigma_\infty 2\pi R_sL+\varepsilon_lL=E_v+E_s+E_l. \quad (4.9)$$

An important point of this kind of models is to make a connection with infinite matter at saturation.[46] If we assume that N helium atoms form a cylinder uniformly filled with density equal to the saturation value ρ_0, then the following relation holds:

$$N=\pi R_0^2L\rho_0. \quad (4.10)$$

As in the spherical case, here one may also introduce a unit radius r_0 satisfying

$$\pi\frac{R_0^2}{N}L\rho_0=\pi r_0^2L\rho_0=1\Rightarrow r_0=\sqrt{\frac{1}{\pi\rho_0L}}. \quad (4.11)$$

On the basis of these relations, the radius R_0 of the cylinder can be written as

$$R_0=r_0N^{1/2}=\sqrt{\frac{1}{\pi\rho_0}}n_\lambda^{1/2}=\eta_0n_\lambda^{1/2}. \quad (4.12)$$

This equation resembles the form $R_0=a_0N^{1/3}$ known from nuclear physics.[45,46] Here we have introduced the longitudinal particle density n_λ defined as the number of particles per unit length of the cylinder

$$n_\lambda=\frac{N}{L}=2\pi\int_0^{\infty}r\,dr\,\rho(r). \quad (4.13)$$

Since this quantity accounts for the radial size of the cylinder, it becomes plausible to expect that it should be the expanding parameter.

In fact, for a cylinder with finite radius the central density along the principal axis ρ_c will, in general, be different from ρ_0. Therefore, it becomes useful to define the relative compression variable ϵ by

$$\epsilon=\frac{\delta\rho}{\rho_0}=\frac{\rho_c-\rho_0}{\rho_0}=\frac{R_0^2}{R_s^2}-1, \quad (4.14)$$

where Eqs. (4.4) and (4.10) have been used for expressing densities in terms of the radii. This relation allows us to express R_s in terms of R_0 and ϵ,

$$R_s=R_0\sqrt{\frac{1}{1+\epsilon}}=\sqrt{\frac{N}{\pi\rho_0L}}\left[1-\frac{1}{2}\epsilon+O(\epsilon^2)\right]$$

$$=\sqrt{\frac{1}{\pi\rho_0}}\left(1-\frac{\epsilon}{2}\right)n_\lambda^{1/2}$$

$$=\eta_0\left(1-\frac{\epsilon}{2}\right)n_\lambda^{1/2}. \quad (4.15)$$

In this macroscopic model, in order to write down the energy per particle e in terms of n_λ, one must first estimate ϵ. Keeping in mind that the latter quantity is essentially the density at the principal axis of the cylinder it may be determined variationally by requiring that e be a minimum at the optimal ϵ. For a system of given length L and number of particles N (i.e., at fixed n_λ) this condition reads

$$\frac{\partial}{\partial\epsilon}\left(\frac{E_{\rm gs}}{N}\right)_{L,N}=0, \quad (4.16)$$

and resembles the EL Eq. (1.4) formulated for getting $\rho(\mathbf{r})$. It should be noticed that this procedure has been applied in the past for studying spherical drops (see, e.g., Sec. 2 of Ref. 46). Now, one should express the quantities involved in Eq. (4.9) keeping the lowest-order contributions carried by ϵ. For uniform systems with ρ_c close to ρ_0, the evaluation of the volume energy E_v in the DM leads to Eq. (3) of Ref. 46, i.e.,

$$E_v=e_cN=e_\infty N+\frac{1}{2}\mathcal{K}N\epsilon^2, \quad (4.17)$$

where $e_\infty=e_B=-7.15$ K is the energy per particle of infinite uniform helium matter at saturation and $\mathcal{K}=27.2$ K the corresponding coefficient of incompressibility (values same as those quoted in Table I). The contribution E_s is the cost in energy to form the lateral surface of a large cylinder. According to Eq. (4.9) it is equal to the asymptotic surface tension σ_∞ multiplied by the lateral area of the cylinder $A=2\pi R_sL$. Upon introducing the expression (4.15) for the sharp mean radius, one arrives at

$$E_s=\sigma_\infty 2\pi R_sL=2\sigma_\infty\sqrt{\frac{\pi LN}{\rho_0}}\left(1-\frac{\epsilon}{2}\right). \quad (4.18)$$

In this approach one assumes that the contribution $E_l=\varepsilon_lL$ is independent of ϵ. So, the ground-state energy per particle of a large cylindrical system of N particles may be written as

$$\frac{E_{\rm gs}}{N}=e_\infty+\frac{\mathcal{K}}{2}\epsilon^2+2\sigma_\infty\sqrt{\frac{\pi}{\rho_0}}\left(1-\frac{\epsilon}{2}\right)n_\lambda^{-1/2}+\varepsilon_ln_\lambda^{-1}. \quad (4.19)$$

Upon imposing Eq. (4.16) the relative compression ϵ is obtained from

$$\frac{\partial}{\partial \epsilon}\left(\frac{E_{\rm gs}}{N}\right)_{L,N} = \mathcal{K}\epsilon - \sigma_\infty \sqrt{\frac{\pi}{\rho_0}} n_\lambda^{-1/2} = 0, \tag{4.20}$$

which yields

$$\epsilon = \frac{\rho_c - \rho_0}{\rho_0} = \frac{\sigma_\infty}{\mathcal{K}} \sqrt{\frac{\pi}{\rho_0}} n_\lambda^{-1/2}. \tag{4.21}$$

This formula predicts a squeezing effect for large cylindrical systems, manifested by the fact that the central density is bigger than the saturation density of infinite helium matter, $\rho_c > \rho_0$. This phenomenon has been already found in calculations carried out for spherical clusters of ^{4}He (see, Fig. 3 of Ref. 18) and is known as the ''leptodermous'' behavior. The squeezing effect, i.e., the difference $\rho_c - \rho_0$, vanishes for $n_\lambda \to \infty$.

Taking into account all the results given in the previous paragraphs the ground-state energy per particle becomes

$$e = \frac{E_{\rm gs}}{N} = \frac{E_{\rm gs}}{n_\lambda L} = e_\infty + 2\sigma_\infty \sqrt{\frac{\pi}{\rho_0}} n_\lambda^{-1/2} + \left(\varepsilon_l - \frac{\pi \sigma_\infty^2}{2\rho_0 \mathcal{K}}\right) n_\lambda^{-1}. \tag{4.22}$$

This equation confirms that $\nu = n_\lambda^{-1/2}$ is the suitable parameter for the expansion and satisfies the condition that the energy per particle in the limit $n_\lambda \to \infty$ should attain e_B of bulk liquid. It is worthy of notice that this polynomial expansion is equivalent to that written in terms of $N^{-1/3}$ for helium drops [see, e.g., Eq. (13) of Ref. 18]. Perhaps it is pertinent to mention that for planar films one expands e as a polynomial in powers of the inverse of coverage $n_c = N/A$ (here A is the area of the planar surface).[47] By keeping in Eq. (4.22) only the first two terms one recovers the asymptotic expression of Eq. (3.1) obtained in Ref. 37.

Let us now add to the ground-state energy of Eq. (4.9) the term stemming from the interaction with a substrate

$$E_{\rm sub} = 2\pi L \int_0^{R_p} r\, dr\, \rho(r) U_{\rm sub}(r). \tag{4.23}$$

We shall treat this contribution as a perturbation to the cylindrical DM formulated above. The simplest way of evaluating this integral is to assume that all N particles are contained in a sharp cylinder of radius R_s with a uniform density distribution ρ_c. In this approach the energy per unit length L is

$$\frac{E_{\rm sub}}{L} = 2\pi \rho_c \int_0^{R_s} r\, dr\, U_{\rm sub}(r), \tag{4.24}$$

while the energy per particle becomes

$$\frac{E_{\rm sub}}{N} = \frac{2}{R_s^2} \int_0^{R_s} r\, dr\, U_{\rm sub}(r). \tag{4.25}$$

The lowest-order approximation for R_s given by Eq. (4.15) leads to

$$\frac{E_{\rm sub}}{N} = 2\pi \rho_0 \left[\int_0^{R_0} r\, dr\, U_{\rm sub}(r)\right] n_\lambda^{-1}. \tag{4.26}$$

Hence, the total e takes the form

$$e = \frac{E_{\rm gs}}{N} = \frac{E_{\rm gs}}{n_\lambda L} = e_\infty + 2\sigma_\infty \sqrt{\frac{\pi}{\rho_0}} n_\lambda^{-1/2} + \left\{\varepsilon_l - \frac{\pi \sigma_\infty^2}{2\rho_0 \mathcal{K}} + 2\pi\rho_0 \int_0^{R_0} r\, dr\, U_{\rm sub}(r)\right\} n_\lambda^{-1}. \tag{4.27}$$

V. THERMODYNAMIC PROPERTIES

A stability condition suitable to be applied in the case of the parametrization of Eq. (4.22) may be derived from thermodynamic considerations. For a single-component system of N particles that presents a volume V and a surface of area A, the ground-state energy at $T = 0$ K satisfies according to Eq. (2.11) of Ref. 48

$$dE_{\rm gs} = -P\, dV + \sigma_A dA + \mu\, dN. \tag{5.1}$$

The intensive thermodynamic fields P, σ_A, and μ are pressure, surface tension, and chemical potential, respectively. The differential changes of volume and area caused by a displacement of the surface parallel to the normal together with an elongation parallel to the axis z are

$$dV = 2\pi R_s L\, dR_s + \pi R_s^2 dL, \tag{5.2}$$

and

$$dA = 2\pi L\, dR_s + 2\pi R_s dL. \tag{5.3}$$

Here the radius R_s of the surface of tension is identified with the sharp radius defined in the previous section. By substituting these expressions into Eq. (5.1) one arrives at

$$dE_{\rm gs} = 2\pi L(-PR_s + \sigma_A) dR_s + \pi R_s(-PR_s + 2\sigma_A) dL + \mu\, dN. \tag{5.4}$$

Here, we assume that the surface tension is independent of curvature (see cite 16 in Ref. 3). Also notice that, if the area of both caps of the cylinder $A_c = 2\pi R_s^2$ is included in the calculation, then this result will be recovered upon imposing the condition $R_s \ll L$. Let us now establish a relation among P, σ_A, and R_s for a system with fixed N. In the case of helium clusters, from the fact that a sphere has the minimum surface area and hence the lowest surface energy, one infers that the equilibrium shape should be spherical. So, for such a geometry, from the condition that work of a virtual increase of the radius vanishes one obtains a relation between the pressure and the surface tension [see, e.g., Eq. (5.26) in Ref. 49]. Extending this idea to a cylindrical geometry, since a circular contour gives the minimum lateral surface and hence the minimum surface energy, a circular section should be the equilibrium shape. By imposing that work of a virtual increase dR_s in the radius should vanish one gets

$$\left(\frac{\partial E_{\rm gs}}{\partial R_s}\right)_{L,N} = 2\pi L(-PR_s + \sigma_A) = 0 \Rightarrow \sigma_A = R_s P. \tag{5.5}$$

This relation obtained for cylindrical systems is equivalent to that valid for spherical droplets[49] and it corresponds to the Laplace's result for a two-dimensional space [see Eq. (2.1) in Ref. 48]. By inputting this result into Eq. (5.4) one arrives at

$$dE_{\rm gs}=\pi R_s\sigma_A dL+\mu\, dN. \tag{5.6}$$

The formal thermodynamic definitions of σ_A and μ lead to the following expressions in terms of the energy per particle e:

$$\pi R_s\sigma_A=\left(\frac{\partial E_{\rm gs}}{\partial L}\right)_N=\left(\frac{\partial(E_{\rm gs}/N)}{\partial(L/N)}\right)_N=-n_\lambda^2\frac{\partial e}{\partial n_\lambda}, \tag{5.7}$$

and

$$\mu=\left(\frac{\partial E_{\rm gs}}{\partial N}\right)_L=\left(\frac{\partial(E_{\rm gs}/L)}{\partial(N/L)}\right)_L=e+n_\lambda\frac{\partial e}{\partial n_\lambda}. \tag{5.8}$$

From these equations one gets the relation

$$\pi R_s\sigma_A=n_\lambda(e-\mu)=\frac{E_{\rm gs}-\mu N}{L}=\frac{\Omega}{L}. \tag{5.9}$$

The chemical potential evaluated by operating with Eq. (5.8) on the expansion (4.27) is

$$\mu=e_\infty+\sigma_\infty\sqrt{\frac{\pi}{\rho_0}}n_\lambda^{-1/2}+2\pi\rho_0\frac{\partial}{\partial n_\lambda}\left[\int_0^{R_0}r\,dr\,U_{\rm sub}(r)\right], \tag{5.10}$$

note that there is no explicit contribution proportional to n_λ^{-1}. The surface tension σ_A at the liquid-vacuum interface derived by using either the definition (5.7) or the relation (5.9) becomes

$$\begin{aligned}\pi R_s\sigma_A=&\sigma_\infty\sqrt{\frac{\pi}{\rho_0}}n_\lambda^{1/2}+\left(\varepsilon_l-\frac{\pi\sigma_\infty^2}{2\rho_0\mathcal{K}}\right)\\&+2\pi\rho_0\int_0^{R_0}r\,dr\,U_{\rm sub}(r)\\&-2\pi\rho_0 n_\lambda\frac{\partial}{\partial n_\lambda}\left[\int_0^{R_0}r\,dr\,U_{\rm sub}(r)\right].\end{aligned} \tag{5.11}$$

In order to check the thermodynamic limit we shall set $U_{\rm sub}(r)\equiv 0$, use the relation $R_s=R_0/\sqrt{1+\epsilon}$, and perform an expansion in powers of ϵ. By keeping all terms up to first order in ν one gets

$$\sigma_A=\sigma_\infty+\sqrt{\frac{\rho_0}{\pi}}\varepsilon_l n_\lambda^{-1/2}. \tag{5.12}$$

It is clear that this expression verifies the asymptotic result for free systems $\sigma_A(n_\lambda\to\infty)=\sigma_\infty$.

A stable configuration must be robust against surface long-wavelength fluctuations along the direction of the principal axis. Following the idea developed in Refs. 14 and 27 for treating planar films, a formulation of a stability criterion for cylindrical systems must require a positive longitudinal isothermal compressibility κ_λ. At $T=0$ K, this condition leads to

$$\begin{aligned}\frac{1}{\kappa_\lambda}&=L\left(\frac{\partial(\pi R_s\sigma_A)}{\partial L}\right)_N=\frac{L}{N}\left(\frac{\partial(\pi R_s\sigma_A)}{\partial(L/N)}\right)_N\\&=-n_\lambda\frac{\partial(\pi R_s\sigma_A)}{\partial n_\lambda}>0.\end{aligned} \tag{5.13}$$

Upon introducing the incompressibility, which has the dimension of an energy, and taking into account Eqs. (5.7) and (5.8) the inequality (5.13) becomes

$$\frac{1}{n_\lambda\kappa_\lambda}=-\frac{\partial(\pi R_s\sigma_A)}{\partial n_\lambda}=n_\lambda\frac{\partial\mu}{\partial n_\lambda}>0, \tag{5.14}$$

in agreement with the necessary condition mentioned in Sec. I. After a straightforward calculation it may be expressed as

$$\begin{aligned}n_\lambda\frac{\partial\mu}{\partial n_\lambda}=&-\frac{\sigma_\infty}{2}\sqrt{\frac{\pi}{\rho_0}}n_\lambda^{-1/2}+2\pi\rho_0 n_\lambda\\&\times\frac{\partial^2}{\partial n_\lambda^2}\left[\int_0^{R_0}r\,dr\,U_{\rm sub}(r)\right]>0.\end{aligned} \tag{5.15}$$

This condition is enough for insure metastable systems. Since for $n_\lambda\to 0$ quantity Ω/L goes to zero, in order to guarantee the stability of a system at finite n_λ one must also require at least $\Omega/L<0$.

It should be mentioned that the condition of Eq. (5.15) may be also obtained on the basis of general grounds. The explicit requirement that the grand thermodynamic potential of Eq. (1.2) must be a minimum implies that besides Eq. (1.3) it should be also satisfied

$$\left(\frac{\partial^2\Omega}{\partial N^2}\right)_\mu=\frac{\partial^2 E_{\rm gs}}{\partial N^2}>0. \tag{5.16}$$

The use of Eqs. (1.3) and (5.16) together with $E_{\rm gs}$ given by the sum of Eqs. (4.9) and (4.26) yields

$$\frac{\partial\mu}{\partial N}=\frac{\partial^2 E_{\rm gs}}{\partial N^2}=\frac{\partial^2}{\partial N^2}[E_v+E_s+E_{\rm sub}]>0. \tag{5.17}$$

By taking into account some relations derived in Sec. IV it is possible to demonstrate that this criterion reduces to that of Eq. (5.15).

Furthermore, according to Eq. (5.3) of Ref. 32 it holds

$$N\frac{\partial\mu}{\partial N}=n_\lambda\frac{\partial\mu}{\partial n_\lambda}=mc_L^2, \tag{5.18}$$

where c_L may be identified with the speed of a longitudinal sound. This kind of sound is a surface wave of the superfluid ^{4}He moving parallel to the z axis resembling the third sound of planar systems.

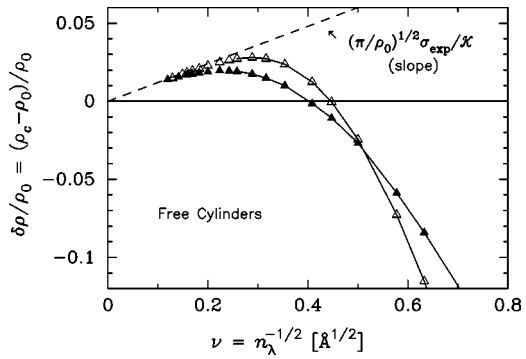

FIG. 6. Relative compression of the central density as a function of the inverse of square root of longitudinal density $\nu = n_\lambda^{-1/2}$. Open and full triangles stand for Skyrme-DF and OP-NLDF results, respectively. The dashed line corresponds to the asymptotic law for $\delta\rho/\rho_0$ [see Eq. (4.21)] with $\sigma_\infty = \sigma_{exp} = 0.272$ K/Å^2 taken from Ref. 40. The solid curves are only given to guide the eye.

VI. ANALYSIS AND DISCUSSION

Let us first center the attention on results for free cylinders. The relative compression at the center of the free cylinders ϵ is plotted as a function of $\nu = n_\lambda^{-1/2}$ in Fig. 6. Small systems with $n_\lambda \lesssim 6$ Å^{-1} ($\nu \gtrsim 0.4$ Å$^{1/2}$) exhibit a central density ρ_c lower than the bulk saturation value ρ_0. This feature has been previously observed in the case of small helium droplets[18] and in the literature it is denoted ''pachydermous'' behavior. For wider cylinders we obtained $\rho_c > \rho_0$. This ''leptodermous'' behavior have been also found in studies of large helium drops (see Fig. 3 in Ref. 18) and of atomic nuclei [see Fig. 1(a) and Fig. 1(b) in Ref. 46], while it is not exhibited by free planar systems of ^{4}He.[50] It is worthy of notice that for cylinders with $\nu \lesssim 0.15$ Å$^{1/2}$ ($n_\lambda \gtrsim 40$ Å^{-1}) the values of ϵ yielded by the solutions of Eq. (2.1) merge into the asymptotic law given by Eq. (4.21). In fact, from values of the relative compression displayed in Fig. 6 it is clear that the largest systems examined in the present work have, in practice, reached the asymptotic behavior.

The results concerning the long-wavelength stability of the free systems can be summarized in the following way. From Fig. 1 one realizes that μ increases monotonically as a function of $n_\lambda^{-1/2}$. In turn, this positive slope of μ vs $n_\lambda^{-1/2}$ implies that the stability condition of Eq. (5.14) is not satisfied by any free cylinder of ^{4}He because one always gets

$$n_\lambda \frac{\partial \mu}{\partial n_\lambda} = -\frac{n_\lambda^{-1/2}}{2} \frac{\partial \mu}{\partial n_\lambda^{-1/2}} < 0. \tag{6.1}$$

Both utilized DF approaches led to the long-wavelength instability of this configuration.

Turning to ^{4}He adsorbed into Cs nanopores we shall first look at the results for the pore of $R_p = 50$ Å. In this case, in order to avoid the crowding of the plot, we only report the outputs from the OP-NLDF approach. Figure 5 shows that for $\nu \gtrsim 0.16$ Å$^{1/2}$ ($n_\lambda \lesssim 40$ Å^{-1}) the values of e and μ lie along the asymptotic lines derived for free systems. Since these data exhibit a positive slope of μ as a function of $n_\lambda^{-1/2}$, according to Eq. (6.1) these systems are unstable. For larger n_λ it begins the filling of the region where the potential presents its well and the systems become even more unstable. At $\nu \simeq 0.10$ Å$^{1/2}$ ($n_\lambda \simeq 100$ Å^{-1}) the slope of μ becomes negative indicating the beginning of a metastable regime. This regime is extended up to the critical value $\nu \simeq 0.088$ Å$^{1/2}$ ($n_\lambda \simeq 130$ Å^{-1}), where Ω/L becomes negative indicating that larger systems of ^{4}He are stable.[14,15] Note that this crossing of e and μ occurs just at the minimum of e in agreement with Eqs. (5.8) and (5.9). An estimation of e can be done by adding the contribution E_{sub}/N given by Eq. (4.26) to the asymptotic form (3.1) obtained for free systems

$$e = e_\infty + 2\sigma_\infty \sqrt{\frac{\pi}{\rho_0}} n_\lambda^{-1/2} + 2\pi\rho_0 \left[\int_0^{R_0} r\, dr\, U_{sub}(r) \right] n_\lambda^{-1}, \tag{6.2}$$

which is a simplified version of Eq. (4.27). The solid curve in Fig. 5 indicates that this approach reproduces satisfactorily well the behavior of e.

Figure 5 shows that for $R_p = 30$ Å the data always show a noticeable departure from the asymptotic values of free cylinders. However, the slopes of e and μ for $\nu \gtrsim 0.30$ Å$^{1/2}$ ($n_\lambda \lesssim 11$ Å^{-1}) differ very little from the free case. For larger systems all the features found for the broader pore occur more rapidly and are more pronounced. At $\nu \simeq 0.20$ Å$^{1/2}$ ($n_\lambda \simeq 25$ Å^{-1}) the slope of μ changes its sign and the systems enter in the metastable regime. The region of stable systems is reached at the critical value $\nu \simeq 0.164$ Å$^{1/2}$ ($n_\lambda \simeq 37$ Å^{-1}) where Ω/L becomes negative. As in the previous case, the solid curve in Fig. 5 stands for e yielded by Eq. (6.2). One realizes that this approximation accounts fairly well for e obtained from the solutions of Eq. (2.1). The most important difference is that the minimum given by Eq. (4.27) is about 1 K too low. However, it is possible to improve the estimation of E_{sub} by taking into account that the density of the liquid does not change abruptly but changes continuously from density liquid to zero over a distance of about $W \simeq 6.5$ Å.[28,51] Assuming a linear fall of the density over the distance W one gets

$$\frac{E_{sub}}{N} = 2\pi\rho_0 \left\{ \int_0^{R_0 - W/2} r\, dr\, U_{sub}(r) + \int_{R_0 - W/2}^{R_0 + W/2} r\, dr \left[\frac{1}{2} + \frac{R_0 - r}{W} \right] U_{sub}(r) \right\} n_\lambda^{-1}. \tag{6.3}$$

As shown in Fig. 7, the use of this expression instead of Eq. (4.25) significantly improves the agreement between e yielded by the DF approaches and the DM. Now, besides accounting for the location of the minimum of e, the model also provides a good value for the minimum.

A few selected density profiles corresponding to different situations in both pores are shown in Fig. 3. In the freelike regime the systems do not show any relevant difference with respect to the free case. Only the central densities exhibit a somewhat enlarged squeezing effect due to the confinement. A connection between data of Figs. 3 and 5 indicates that for

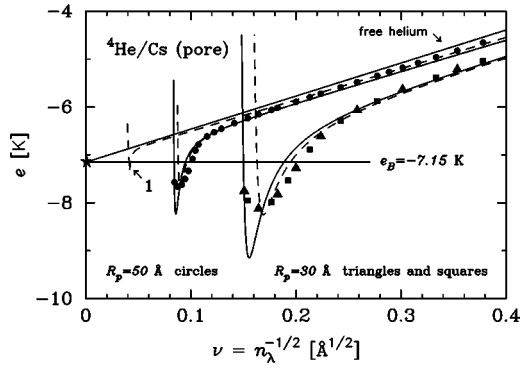

FIG. 7. Similar to Fig. 5. In addition, the dashed curves show the results of the DM with $E_{\rm sub}/N$ given by Eq. (6.3), the label 1 indicates the prediction for a Cs nanopore of $R_p=100$ Å.

both pores the stable regime is reached when the cavities are completely filled with helium. Furthermore, Fig. 3 shows that the density profile of stable systems is everywhere slightly larger than ρ_0 except quite near the wall where there is a strong repulsion.

There is an alternative way for determining the transition to stable CC liquid. From Fig. 4 one realizes that the dependence of μ on n_λ is nonmonotonic. This indicates the presence of a phase transition, requiring a Maxwell construction to find the equilibrium behavior in the same way as in Fig. 6 of Ref. 44. The determined adsorption isotherms are displayed in Fig. 8. This drawing shows that n_λ jumps from zero to the critical value corresponding to a CC liquid which fills the pore. These adsorption isotherms are similar to that of Fig. 3 in Ref. 44 obtained in the case of ^{3}He confined by planar walls of Cs. It should be noticed that the stable CC phase is obtained when n_λ reaches approximately the value

$$n_\lambda^{CCo}=\pi R_{\rm rep}^2\rho_0\,, \tag{6.4}$$

corresponding to a cylindrical cavity of radius $R_{\rm rep}=R_p-5.6$ Å completely filled with liquid of density ρ_0. No stable liquid films (cylindrical shell phase) are obtained. This feature is similar to that found in Ref. 44 for ^{4}He confined

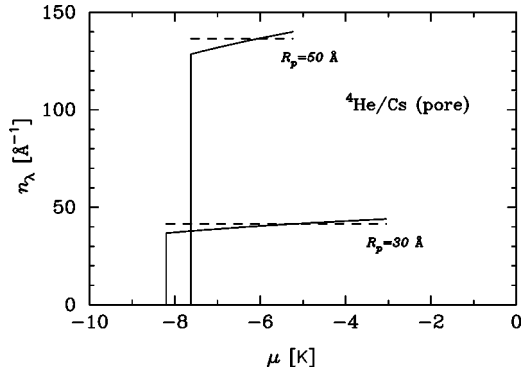

FIG. 8. Longitudinal density as a function of the chemical potential for ^{4}He in cylindrical pores of radii $R_p=30$ and 50 Å in Cs. The solid curves are adsorption isotherms derived from data in Fig. 4 by Maxwell constructions as discussed in the text. The dashed lines are the values of n_λ^{CCo} given by Eq. (6.4).

by parallel walls of Cs at $T=0$ K (see Fig. 13 therein). Therefore, no hysteresis loop like that exhibited in Fig. 6 of Ref. 3 or in Fig. 9 of Ref. 4 was determined.

Perhaps, it is worthwhile to notice that the pores in Cs examined in the present work have an intermediate size. They are one order of magnitude smaller than those in Vycor (nominal radii 15–100 nm) analyzed in Ref. 4 and are somewhat larger than the carbon nanotubes (radius 0.6–0.8 nm) studied in Ref. 9. Let us look for what is going on when the radius of the pore in Cs is increased. Figure 7 shows the values of e yielded by the DM with $E_{\rm sub}$ given by Eq. (6.3) in the case of a cavity with $R_p=10$ nm. This estimation indicates a large freelike regime and an abrupt change to a stable situation. If the radius of the pore is decreased to about $R_p=1$ nm, then due to the large core radius σ_{LJ} of the He-Cs potential ($\simeq$0.65 nm) $U_{\rm sub}(r)$ tends to take the form of a potential well in agreement with the trend as a function of R_p/σ_{LJ} depicted in Fig. 1 of Ref. 6. However, under such conditions, because of the large lattice constant $a=6.045$ Å our procedure for determining $U_{\rm sub}(r)$ would become too poor due to curvature effects.

VII. SUMMARY

The energetics and long-wavelength stability of liquid ^{4}He systems with cylindrical shape were theoretically studied. The calculations were carried out by using zero- and finite-range density functionals. In order to interpret the numerical results we developed a formalism analogous to the DM. It is shown that an expansion of the energy per particle in terms of $n_\lambda^{-1/2}$ is appropriate to account for the behavior yielded by DF calculations. This expansion is valid for cylindrical systems of ^{4}He as well as of ^{3}He, exactly in the same manner like the expansion in terms of $N^{-1/3}$ devised for examining the energetics of spherical drops (see, e.g., Ref. 18). It is demonstrated that a necessary condition for the stability of cylindrical systems is to require a positive derivative of the chemical potential with respect to n_λ. It should be stressed that stable systems must also satisfy $\Omega/L<0$.

Free ^{4}He cylinders exhibit, as shown in Fig. 1, a remarkably good agreement between the values of e and μ provided by DF calculations and those predicted by the DM. For $n_\lambda>40$ Å^{-1} the obtained squeezing effect merges into the asymptotic form for ϵ given by the DM. All these facts indicate that the largest free cylinders have already reached the asymptotic behavior. Since the results plotted in Fig. 1 do not satisfy the stability condition of Eq. (5.15), these systems are unstable just like free planar films. To our knowledge, this is the first microscopic proof of the long-wavelength instability of free cylinders of ^{4}He.

The behaviors of ^{4}He adsorbed into Cs pores of different radii, $R_p=30$ and 50 Å, present some differences as shown in Figs. 5 and 7. For instance, for the smaller pore the results for e and μ exhibit a noticeable deviation from the freelike regime. However, this feature can be understood in terms of the DM when the $E_{\rm sub}$ contribution is taken into account. The stability of the systems is reached when the pores are completely full of helium. This entrance to the stable regime is also well predicted by the DM. An alternative way for deter-

mining the transition to the CC phase is to construct the adsorption isotherms from data of Fig. 4. Such a procedure yields critical values for n_λ consistent with that provided by the DM model.

Let us also notice that for the systems treated in the present work no important differences were found between results yielded by the zero- and finite-range DF approaches. This is due to the fact that, because of the weakness of the pore potential considered, the density profiles do not exhibit oscillations.

Concerning future work, we are undertaking a project to extend this kind of analysis to pores in lighter, more attractive alkali metals, with a possible extension to finite temperature. It is encouraging the fact that Figs. 14 and 15 in Ref. 44 indicate that in the case of slab geometry substrates of Na and Li support stable film configurations. Since the depth of the adsorption potential increases with temperature, finite temperature effects may also favor the formation of stable liquid shell configurations in heavier alkalis.

ACKNOWLEDGMENTS

We wish to thank M. W. Cole and E. S. Hernández for enlightening and fruitful discussions. This work was supported in part by the Ministry of Culture and Education of Argentina through CONICET Contract No. PIP-4486/96; ANPCYT Grant PICT-1706; and under SIP Grants Nos. EX-01/TX55, EX-01/TW81, and EX-X/103.

APPENDIX: HARTREE MEAN-FIELD POTENTIALS

In this Appendix we summarize the expressions needed for treating cylindrical systems characterized by the polar coordinates r, φ, and z.

The Hartree mean-field potential derived by using the definition of Eq. (2.2) in the case of the Skyrmelike DF reads

$$V_H^{\mathrm{Sky}}(r)=b_4\rho(r)+\frac{\gamma_4+2}{2}c_4\rho^{\gamma_4+1}(r)-2d_4\times\left(\frac{d^2}{dr^2}+\frac{1}{r}\frac{d}{dr}\right)\rho(r). \tag{A1}$$

In the OP-NLDF approach the correlation energy per particle is

$$e_{sc}^{\mathrm{OP}}(r)=4\int_0^\infty r'dr'\rho(r')\int_0^\pi d\varphi\int_0^\infty dz'V_l^{\mathrm{OP}}(R)+\frac{c_4}{2}[\overline{\rho}(r)]^{\gamma_4+1}, \tag{A2}$$

where R is the distance between two particles located at $\mathbf{r}$ and $\mathbf{r}'$

$$R^2=|\mathbf{r}-\mathbf{r}'|^2=z'^2+\eta^2, \tag{A3}$$

with η being the distance R projected onto the polar plane perpendicular to the z' axis

$$\eta^2=r^2+r'^2-2rr'\cos\varphi. \tag{A4}$$

The Hartree potential obtained according to Eq. (2.2) is

$$V_H^{\mathrm{OP}}(r)=\frac{\delta E_{sc}[\rho]}{\delta\rho(r)}=\int d\mathbf{r}'\rho(r')V_l^{\mathrm{OP}}(|\mathbf{r}-\mathbf{r}'|)+\frac{c_4}{2}[\overline{\rho}(r)]^{\gamma_4+1}+\frac{c_4}{2}(\gamma_4+1)\times\int d\mathbf{r}'\rho(r')[\overline{\rho}(r')]^{\gamma_4}\mathcal{W}(|\mathbf{r}-\mathbf{r}'|). \tag{A5}$$

Here we shall provide the expressions derived in the present work for the contributions involving the ''coarse-grained weight,'' i.e.,

$$\overline{\rho}(r)=\int d\mathbf{r}'\rho(r')\mathcal{W}(|\mathbf{r}-\mathbf{r}'|), \tag{A6}$$

and

$$\overline{\rho}_V(r)=\int d\mathbf{r}'\rho(r')[\overline{\rho}(r')]^{\gamma_4}\mathcal{W}(|\mathbf{r}-\mathbf{r}'|), \tag{A7}$$

with

$$\mathcal{W}(|\mathbf{r}-\mathbf{r}'|)=\frac{3}{4\pi h_{\mathrm{OP}}^3}\Theta(h_{\mathrm{OP}}-|\mathbf{r}-\mathbf{r}'|)=\begin{cases}\dfrac{3}{4\pi h_{\mathrm{OP}}^3}, & \text{if } |\mathbf{r}-\mathbf{r}'|\leqslant h_{\mathrm{OP}},\\ 0, & \text{if } |\mathbf{r}-\mathbf{r}'|>h_{\mathrm{OP}}.\end{cases} \tag{A8}$$

Both these integrals may be cast into the form

$$\overline{\mathcal{R}}(r)=\frac{3}{4\pi h_{\mathrm{OP}}^3}\int d\mathbf{r}'\mathcal{R}(r')\Theta(h_{\mathrm{OP}}-|\mathbf{r}-\mathbf{r}'|). \tag{A9}$$

After introducing cylindrical coordinates and taking into account that the step function is symmetric in the azimuthal angle φ and in the z' coordinate along the principal axis, the integration over the latter variable yields

$$\begin{aligned}\overline{\mathcal{R}}(r)&=\frac{3}{\pi h_{\mathrm{OP}}^3}\int_{r'_{\min}}^{r'_{\max}}r'\,dr'\mathcal{R}(r')\int_0^{\varphi_{\max}}d\varphi\times\int_0^{z'_{\max}}dz'\Theta[h_{\mathrm{OP}}^2-z'^2-r^2-r'^2+2rr'\cos\varphi]\\&=\frac{3}{\pi h_{\mathrm{OP}}^3}\int_{r'_{\min}}^{r'_{\max}}r'dr'\mathcal{R}(r')\times\int_0^{\varphi_{\max}}d\varphi\sqrt{h_{\mathrm{OP}}^2-r^2-r'^2+2rr'\cos\varphi}.\end{aligned} \tag{A10}$$

For points located at $r=0$ one gets

$$\overline{\mathcal{R}}(r=0)=\frac{3}{h_{\mathrm{OP}}^3}\int_0^{h_{\mathrm{OP}}} r'\,dr'\,\mathcal{R}(r')\sqrt{h_{\mathrm{OP}}^2-r'^2}. \quad \text{(A11)}$$

For $r>0$ two different cases should be considered: (i) $0<r\leqslant h_{\mathrm{OP}}$ and (ii) $r>h_{\mathrm{OP}}$. For $0<r\leqslant h_{\mathrm{OP}}$ the integral over r' should be split into two parts

$$\overline{\mathcal{R}}(r)=\frac{3}{\pi h_{\mathrm{OP}}^3}\left\{\int_0^{h_{\mathrm{OP}}-r}+\int_{h_{\mathrm{OP}}-r}^{r+h_{\mathrm{OP}}}\right\} r'\,dr'\,\mathcal{R}(r')\int_0^{\varphi_{\max}} d\varphi \times\sqrt{h_{\mathrm{OP}}^2-r^2-r'^2+2rr'\cos\varphi}. \quad \text{(A12)}$$

Since for the first integral over r' the upper angular limit is $\varphi_{\max}=\pi$, while for the second integral $\varphi_{\max}$ is determined by the condition

$$h_{\mathrm{OP}}^2=r^2+r'^2-2rr'\cos\varphi_{\max}, \quad \text{(A13)}$$

then

$$\overline{\mathcal{R}}(r)=\frac{3}{\pi h_{\mathrm{OP}}^3}\int_0^{h_{\mathrm{OP}}-r} dr'\,r'\mathcal{R}(r') \times\int_0^{\pi} d\varphi\sqrt{h_{\mathrm{OP}}^2-r^2-r'^2+2rr'\cos\varphi} + \frac{3\sqrt{2r}}{\pi h_{\mathrm{OP}}^3}\int_{h_{\mathrm{OP}}-r}^{r+h_{\mathrm{OP}}} dr'\,r'^{3/2}\,\mathcal{R}(r') \times\int_0^{\varphi_{\max}} d\varphi\sqrt{\cos\varphi-\cos\varphi_{\max}}. \quad \text{(A14)}$$

The integration over φ leads to elliptic integrals giving rise to hypergeometric functions F,

$$\overline{\mathcal{R}}(r)=\frac{3}{h_{\mathrm{OP}}^3}\int_0^{h_{\mathrm{OP}}-r} r'\,dr'\,\mathcal{R}(r')\sqrt{h_{\mathrm{OP}}^2-(r'-r)^2} \times F\left(-\frac{1}{2},\frac{1}{2};1;1/a^2\right)+\frac{6\sqrt{r}}{h_{\mathrm{OP}}^3}\int_{h_{\mathrm{OP}}-r}^{r+h_{\mathrm{OP}}} dr'\,r'^{3/2}\,\mathcal{R}(r') \times\left[F\left(-\frac{1}{2},\frac{1}{2};1;a^2\right)-(1-a^2)F\left(\frac{1}{2},\frac{1}{2};1;a^2\right)\right], \quad \text{(A15)}$$

where

$$a^2=\sin^2(\varphi_{\max}/2)=\frac{1-\cos\varphi_{\max}}{2}=\frac{h_{\mathrm{OP}}^2-(r'-r)^2}{4rr'}. \quad \text{(A16)}$$

For $r>h_{\mathrm{OP}}$, only the second term in Eq. (A14) contributes

$$\overline{\mathcal{R}}(r)=\frac{3\sqrt{2r}}{\pi h_{\mathrm{OP}}^3}\int_{r-h_{\mathrm{OP}}}^{r+h_{\mathrm{OP}}} dr'\,r'^{3/2}\,\mathcal{R}(r') \times\int_0^{\varphi_{\max}} d\varphi\,\sqrt{\cos\varphi-\cos\varphi_{\max}}, \quad \text{(A17)}$$

leading to

$$\overline{\mathcal{R}}(r)=\frac{6\sqrt{r}}{h_{\mathrm{OP}}^3}\int_{r-h_{\mathrm{OP}}}^{r+h_{\mathrm{OP}}} dr'\,r'^{3/2}\,\mathcal{R}(r')\left[F\left(-\frac{1}{2},\frac{1}{2};1;a^2\right)-(1-a^2)F\left(\frac{1}{2},\frac{1}{2};1;a^2\right)\right], \quad \text{(A18)}$$

with a^2 given by Eq. (A16).

The contribution containing the screened LJ potential

$$V_H^{\mathrm{LJScr}}(r)=\int d\mathbf{r}'\rho(r')V_l^{\mathrm{OP}}(|\mathbf{r}-\mathbf{r}'|) =V_l^{\mathrm{OP}}(h_{\mathrm{OP}})\int_{R\leqslant h_{\mathrm{OP}}} d\mathbf{r}'\rho(r')\left(\frac{R}{h_{\mathrm{OP}}}\right)^4 +4\varepsilon\int_{R\geqslant h_{\mathrm{OP}}} d\mathbf{r}'\rho(r')\left[\left(\frac{\sigma_{LJ}}{R}\right)^{12}-\left(\frac{\sigma_{LJ}}{R}\right)^{6}\right], \quad \text{(A19)}$$

was evaluated in the same way as in Ref. 9.

*Also at the Carrera del Investigador Científico of the Consejo Nacional de Investigaciones Científicas y Técnicas, Av. Rivadavia 1917, RA–1033 Buenos Aires, Argentina.

[1] K. R. Atkins, H. Seki, and E. U. Condon, Phys. Rev. **102**, 582 (1956).
[2] M. W. Cole and W. F. Saam, Phys. Rev. Lett. **32**, 985 (1974).
[3] W. F. Saam and M. W. Cole, Phys. Rev. B **11**, 1086 (1975).
[4] K. M. Godshalk and R. B. Hallock, Phys. Rev. B **36**, 8294 (1987).
[5] T. W. Ebbesen, Physics Today **49** (6), 26 (1996); M. S. Dresselhaus, G. Dresselhaus, and P. E. Eklund, *Science of Fullerenes and Carbon Nanotubes* (Academic, New York, 1997).
[6] G. Stan and M. W. Cole, Surf. Sci. **395**, 280 (1998).
[7] W. Teizer, R. B. Hallock, E. Dujardin, and T. W. Ebbesen, Phys. Rev. Lett. **82**, 5305 (1999); **84**, 1844(E) (2000).
[8] M. W. Cole, V. H. Crespi, G. Stan, C. Ebner, J. M. Hartman, S. Moroni, and M. Boninsegni, Phys. Rev. Lett. **84**, 3883 (2000).
[9] S. M. Gatica, G. Stan, M. M. Calbi, J. K. Johnson, and M. W. Cole, J. Low Temp. Phys. **120**, 337 (2000).
[10] M. W. Cole, J. Low Temp. Phys. **101**, 25 (1995).
[11] R. B. Hallock, J. Low Temp. Phys. **101**, 31 (1995).
[12] J. A. Phillips, P. Taborek, and J. E. Rutledge, J. Low Temp. Phys. **113**, 829 (1998).

[13] J. A. Phillips, D. Ross, P. Taborek, and J. E. Rutledge, Phys. Rev. B **58**, 3361 (1998).
[14] L. Szybisz, Phys. Rev. B **62**, 3986 (2000).
[15] L. Szybisz, Phys. Rev. B **62**, 12 381 (2000).
[16] F. Ancilotto, F. Faccin, and F. Toigo, Phys. Rev. B **62**, 17 035 (2000).
[17] D. Ross, J. E. Rutledge, and P. Taborek, Science **278**, 664 (1997).
[18] S. Stringari and J. Treiner, J. Chem. Phys. **87**, 5021 (1987).
[19] S. Stringari and J. Treiner, Phys. Rev. B **36**, 8369 (1987).
[20] J. Dupont-Roc, M. Himbert, N. Pavloff, and J. Treiner, J. Low Temp. Phys. **81**, 31 (1990).
[21] E. Cheng, M. W. Cole, W. F. Saam, and J. Treiner, Phys. Rev. B **46**, 13 967 (1992); **47**, 14 661(E) (1993).
[22] E. Cheng, M. W. Cole, J. Dupont-Roc, W. F. Saam, and J. Treiner, Rev. Mod. Phys. **65**, 557 (1993).
[23] M. Barranco and E. S. Hernández, Phys. Rev. B **49**, 12 078 (1994); S. M. Gatica, E. S. Hernández, and M. Barranco, J. Chem. Phys. **107**, 927 (1997).
[24] F. Dalfovo, A. Lastri, L. Pricaupenko, S. Stringari, and J. Treiner, Phys. Rev. B **52**, 1193 (1995).
[25] A. Lastri, F. Dalfovo, L. Pitaevskii, and S. Stringari, J. Low Temp. Phys. **96**, 227 (1995).
[26] L. Szybisz, Phys. Rev. B **56**, 11 845 (1997).
[27] L. Szybisz, Phys. Rev. B **58**, 109 (1998).
[28] L. Szybisz, Eur. Phys. J. B **14**, 733 (2000).
[29] L. Pricaupenko and J. Treiner, Phys. Rev. Lett. **72**, 2215 (1994).
[30] M. Lewerenz, J. Chem. Phys. **106**, 4596 (1997), and references quoted therein.
[31] S. A. Safran, *Statistical Thermodynamics of Surfaces, Interfaces, and Membranes* (Addison-Wesley, Reading, Massachusetts, 1994), Sec. 3.4.
[32] B. E. Clements, H. Forbert, E. Krotscheck, and M. Saarela, J. Low Temp. Phys. **95**, 849 (1994).
[33] I. E. Dzyaloshinskii, E. M. Lifshitz, and L. P. Pitaevskii, Adv. Phys. **10**, 165 (1961).
[34] J. de Boer and A. Michels, Physica (Amsterdam) **6**, 945 (1938).
[35] J. L. Vallés and K. E. Schmidt, Phys. Rev. B **38**, 2879 (1988).
[36] S. A. Chin and E. Krotscheck, Phys. Rev. B **52**, 10 405 (1995).
[37] L. Szybisz, Physica A **283**, 193 (2000).
[38] H. M. Guo, D. O. Edwards, R. E. Sarwinski, and J. T. Tough, Phys. Rev. Lett. **27**, 1259 (1971); D. O. Edwards and W. F. Saam, in *Progress in Low Temperature Physics*, edited by D. F. Brewer (North-Holland, Amsterdam, 1978), Vol. 7A, Chap. 4.
[39] M. Iino, M. Suzuki, and A. J. Ikushima, J. Low Temp. Phys. **61**, 155 (1985).
[40] P. Roche, G. Deville, N. J. Appleyard, and F. I. B. Williams, J. Low Temp. Phys. **106**, 565 (1997).
[41] F. Ancilotto, E. Cheng, M. W. Cole, and F. Toigo, Z. Phys. B: Condens. Matter **98**, 323 (1995).
[42] S. H. Patil, J. Chem. Phys. **94**, 8089 (1991).
[43] C. Kittel, *Introduction to Solid State Physics* (Wiley, New York, 1986), Chap. 1.
[44] M. M. Calbi, F. Toigo, S. M. Gatica, and M. W. Cole, Phys. Rev. B **60**, 14 935 (1999).
[45] W. D. Myers and W. J. Swiatecki, Ann. Phys. **55**, 395 (1969).
[46] J. Treiner, W. D. Myers, W. J. Swiatecki, and M. S. Weiss, Nucl. Phys. A **452**, 93 (1986).
[47] L. Szybisz, J. Low Temp. Phys. **116**, 215 (1999).
[48] J. S. Rowlinson and B. Widom, *Molecular Theory of Capillarity* (Clarendon Press, Oxford, 1982).
[49] C. Ebner and W. F. Saam, Phys. Rev. B **12**, 923 (1975).
[50] L. Szybisz (unpublished).
[51] J. Harms, J. P. Toennies, and F. Dalfovo, Phys. Rev. B **58**, 3341 (1998).